months, when mussel cover in some replicates approached zero. In each plot, whelk densities were manipulated using 20 cm × 20 cm stainless steel cages attached to the rock. Cages either excluded whelks or enclosed two or six whelks corresponding to a range of densities naturally observed (0, 50 and 150 whelks per m^2, respectively). All treatments were replicated in four large patches in the mid-intertidal mussel bed. One high-density replicate was lost because of winter storm damage. Whelk effects were quantified as the difference in mussel colonization rates (change in per cent cover per month) between −whelk treatments and +whelk treatments (either low or high density). Although the results and conclusions were qualitatively identical when effects were measured using Pain's[6] index (data not shown), I present effect strengths in terms of the difference in colonization rates because this measure, unlike Pain's, does not assume equilibrium prey abundance[16,29].

Factorial experiment. All plots were initially scraped bare and both mussels and barnacles colonized naturally. Whelks were enclosed at three different densities (0, 50 and 150 whelks per m^2) in 20 cm × 20 cm cages, and for each whelk density, barnacles were removed monthly from half the cages. All treatments were initiated in April over three successive years: 1991, 1992 and 1993. The interactive effects of predator density (none, low, high), barnacles (present, absent) and start date (1991, 1992, 1993) on mussel colonization rate was analysed using a randomized block ANOVA. Repeated measures was not used because, although all three experimental runs were initiated over 3 years in the same blocks, individual plot localities differed between years. Data (per cent cover per month) were arcsine (square root)-transformed for analysis.

Received 18 November 1998; accepted 8 February 1999.

1. Paine, R. T. A note on trophic complexity and community stability. *Am. Nat.* **103,** 91–93 (1969).
2. Paine, R. T. Intertidal community structure. Experimental studies on the relationship between a dominant competitor and its principal predator. *Oecologia* **15,** 93–120 (1974).
3. Power, M. E. *et al.* Challenges in the quest for keystones. *BioScience* **46,** 609–620 (1996).
4. Menge, B. A., Berlow, E. L., Blanchette, C., Navarrete, S. A. & Yamada, S. B. The keystone species concept: variation in interaction strength in a rocky intertidal habitat. *Ecol. Monogr.* **64,** 249–286 (1994).
5. Estes, J. A. & Palmisano, J. F. Sea otters: their role in structuring nearshore communities. *Science* **185,** 1058–1060 (1974).
6. Paine, R. T. Food-web analysis through field measurement of per capita interaction strength. *Nature* **355,** 73–75 (1992).
7. Fagan, W. F. & Hurd, L. E. Hatch density variation of a generalist arthropod predator: population consequences and community impact. *Ecology* **75,** 2022–2032 (1994).
8. Raffaelli, D. G. & Hall, S. J. in *Food Webs: Integration of Patterns and Dynamics* (eds Polis, G. & Winemiller, K.) 185–191 (Chapman and Hall, New York, 1995).
9. Wootton, J. T. Estimates and tests of per-capita interaction strength: diet, abundance, and impact of intertidally-foraging birds. *Ecol. Monogr.* **67,** 45–64 (1997).
10. Hooper, D. U. & Vitousek, P. M. The effects of plant composition and diversity on ecosystem processes. *Science* **277,** 1302–1305 (1997).
11. Tilman, D. *et al.* The influence of functional diversity and composition on ecosystem processes. *Science* **277,** 1300–1308 (1997).
12. Wardle, D. A., Zackrisson, O., Hörnbreg, G. & Gallet, C. The influence of island area on ecosystem properties. *Science* **277,** 1296–1299 (1997).
13. Symstad, A. J., Tilman, D., Wilson, J. & Knops, J. M. H. Species loss and ecosystem functioning: effects of species identity and community composition. *Oikos* **81,** 389–397 (1998).
14. Bengtsson, J., Jones, J. & Setälä, H. The value of biodiversity.l *Trends Ecol. Evol.* **12,** 334–336 (1997).
15. McGrady-Steed, J., Harris, P. M. & Morin, P. J. Biodiversity regulates ecosystem predictabiity. *Nature* **390,** 162–165 (1997).
16. Berlow, E. L., Navarrete, S. A., Briggs, C. J., Power, M. E. & Menge, B. A. Quantifying variation in the strengths of species interactions. *Ecology* (in the press).
17. McCann, K., Hastings, A. & Huxel, G. R. Weak trophic interactions and the balance of nature. *Nature* **395,** 794–798 (1998).
18. Polis, G. A. & Strong, D. R. Food web complexity and community dynamics. *Am. Nat.* **147,** 813–846 (1996).
19. Chapin, F. S., Lubchenco, J. & Reynolds, H. J. in *Global Biodiversity Assessment, United Nations Environmental Programme* (eds Heywood, V. H. & Watson, R. T.) Chapter 5.2.2 (Cambridge Univ. Press, Cambridge, 1995).
20. Lawton, J. H. & Brown, V. K. in *Biodiversity and Ecosystem Function* (eds Schultze, E. D. & Mooney, H. A.) 255–270 (Springer, Berlin, 1993).
21. Naeem, S. & Li, S. Biodiversity enhances ecosystem reliability. *Nature* **390,** 507–509 (1997).
22. Frost, T. M., Carpenter, S. R., Ives, A. R. & Kratz, T. K. *Linking Species and Ecosystems* (eds Jones, C. G. & Lawton, J. H.) 224–239 (Chapman and Hall, New York, 1995).
23. Navarrete, S. A. & Menge, B. A. Keystone predation and interaction strength: interactive effects of predators on their main prey. *Ecol. Monogr.* **66,** 409–429 (1996).
24. Westman, W. E. Managing for biodiversity: unresolved science and policy questions. *Bioscience* **40,** 26–33 (1990).
25. Berlow, E. L. From canalization to contingency: historic effects in a successional rocky intertidal community. *Ecol. Monogr.* **67,** 435–460 (1997).
26. Paine, R. T. & Levin, S. A. Intertidal landscapes: disturbance and the dynamics of pattern. *Ecol. Monogr.* **51,** 145–178 (1981).
27. Power, M. E. Resource enhancement by indirect effects of grazers: Armored catfish, algae, and sediment. *Ecology* **71,** 897–904 (1990).
28. Navarrete, S. A. Variable predation: effects of whelks on a mid intertidal successional community. *Ecol. Monogr.* **66,** 301–321 (1996).
29. Laska, M. S. & Wootton, J. T. Theoretical concepts and empirical approaches to measuring interaction strength. *Ecology* **79,** 461–476 (1998).

Acknowledgements. I thank K. Buzzard, B. Daley, J. and T. Panek, B. Profit and S. Suskie for assistance in the field, B. and A. King for the use of their front yard, and G. Allison, C. Blanchette, F. S. Chapin, J. Corbin, C. M. D'Antonio, J. Dunne, S. Hobbie, D. Hooper, B. Langford, H. Lefcort, J. Levine, J. Lubchenco, N. D. Martinez, B. McCune, B. Menge, S. Navarrete, R. Paine, I. Parker, M. Power, W. Riley, A. Smyth, P. van Tamelen and J. T. Wootton for invaluable advice during the study. This work was supported in part by the Oregon State University Zoology Research Fund, the Holt Marine Education Fund, Sigma Xi, NSF and the Andrew W. Mellon Foundation. It was also greatly facilitated by the Sierra Nevada Aquatic Research Laboratory and the 1997–98 El Niño.

Correspondence and requests for materials should be addressed to E.L.B. (e-mail: berlow@socrates.berkeley.edu).

Anticipation of moving stimuli by the retina

Michael J. Berry II, Iman H. Brivanlou, Thomas A. Jordan* & Markus Meister

Department of Molecular and Cellular Biology, Harvard University, 16 Divinity Avenue, Cambridge, Massachusetts 02138, USA

A flash of light evokes neural activity in the brain with a delay of 30–100 milliseconds[1], much of which is due to the slow process of visual transduction in photoreceptors[2,3]. A moving object can cover a considerable distance in this time, and should therefore be seen noticeably behind its actual location. As this conflicts with everyday experience, it has been suggested that the visual cortex uses the delayed visual data from the eye to extrapolate the trajectory of a moving object, so that it is perceived at its actual location[4–7]. Here we report that such anticipation of moving stimuli begins in the retina. A moving bar elicits a moving wave of spiking activity in the population of retinal ganglion cells. Rather than lagging behind the visual image, the population activity travels near the leading edge of the moving bar. This response is observed over a wide range of speeds and apparently compensates for the visual response latency. We show how this anticipation follows from known mechanisms of retinal processing.

Because a moving object often follows a smooth trajectory, one can extrapolate from its past position and velocity to obtain an estimate of its current location. Recent experiments on motion perception[5–7] indicate that the human brain possesses just such a mechanism: Subjects were shown a moving bar sweeping at constant velocity; a second bar was flashed briefly in alignment with the moving bar. When asked what they perceived at the time of the flash, observers reliably reported seeing the flashed bar trailing behind the moving bar. This flash lag effect has been confirmed repeatedly[8–10], and various high-level processes have been invoked to explain it, such as a time delay due to the shift of visual attention. To assess whether processing in the retina contributes to this effect we analysed the 'neural image' of these two stimuli at the retinal output. We recorded simultaneously the spike trains of many ganglion cells in the isolated retina of tiger salamander or rabbit. The responses to flashed and moving bars were then analysed by plotting the firing rate in the retinal ganglion-cell population as a function of space and time.

Figure 1 illustrates the responses of individual OFF-type ganglion cells to a dark bar flashed briefly over the receptive-field centre. In both salamander (Fig. 1a) and rabbit (Fig. 1b), the cells remained silent for a latency of ~50 ms, then fired a burst of spikes that lasted another 50 ms. When the bar was swept over the retina at constant speed (Fig. 1c, d), these same cells fired for a more extended period, beginning some time before the bar reached the position at which the flash occurred, and extending for a shorter time thereafter. When the bar was swept in the opposite direction (Fig. 1e, f), it produced a very similar response, showing that these cells had no direction-selective preference.

* Present address: Department of Psychiatry and Behavioral Sciences, Stanford University School of Medicine, Stanford, California 94305, USA.

From many single-unit measurements such as these, we compiled the neural image of the visual stimulus in the population of ganglion cells. This was done by plotting the firing rate of every cell as a function of distance from the bar stimulus and interpolating these points with a smooth line (see Methods). The neural image of the flashed bar among salamander 'fast OFF' cells is shown in Fig. 2a. After a latency of 40 ms, a hump of neural activity appears that increases rapidly to a peak at 60 ms, then declines and disappears at 100 ms. As might be expected, the profile is centred on the bar. It has a width on the retina of ~200 μm at half-maximum, close to the size of the receptive-field centre for these neurons[11]. The width increases somewhat during the late phase of the response, creating the impression of an outward 'splash'[12].

The neural image of the moving bar is shown in Fig. 2b. Again, a hump of firing activity is observed, which now sweeps over the retina along with the moving bar. If this response were subject to the same time delay as the flash, one would expect the neural image to trail behind the visual image of the bar. Instead, the hump of firing activity is clearly ahead of the centre of the bar, and the peak firing rate seems to occur near the bar's leading edge. The same response occurs when the bar moves in the opposite direction. By superposing on this the response to a flash that was aligned with the moving bar (from Fig. 2a), we find that the two neural images are clearly separated—at the time when the response to the flash peaks, the response of the moving bar is displaced ~100 μm ahead in the direction of motion. A very similar displacement between the two neural images was observed among brisk-sustained OFF cells in the rabbit retina (Fig. 2c). If subsequent stages of the visual system estimate the location of the flashed bar and the moving bar by the position of these humps of neural activity, they must conclude that the moving bar is ahead of the flashed bar.

How does this apparent anticipation of the moving bar come about? One suspects that cells ahead of the bar start firing early (Figs 1c–f, 2b, c) when the bar begins to invade their receptive-field centre. The firing profile does not extend to an equal distance behind the trailing edge of the bar, perhaps because these ganglion cells have transient responses: They fire while stimulation increases as the bar invades the receptive field, not while stimulation decreases as the bar leaves it. However, we found that spatial and temporal filtering by the ganglion cell's receptive field was by itself insufficient to explain the response profiles (see below). Instead, there is another important component, which was revealed in experiments varying the intensity of the moving bar.

Figure 3a illustrates the response of this neural population to dark bars of increasing contrast relative to the background. As expected, bars of higher contrast produced stronger modulations in firing. The peak firing rate increased in proportion to contrast at first, but then appeared to saturate (Fig. 3a, inset). In addition, the shape of the neural image changed significantly with contrast. At low contrast, the peak in firing occurred behind the bar's leading edge. At high contrast—the same condition as in Fig. 2—the peak of the profile was ahead of the leading edge, followed by a more gradual decline in firing. The saturation of the peak firing rate and the shift in the response profile can be explained if the high-contrast stimulus somehow desensitizes the response of the ganglion cell after a short

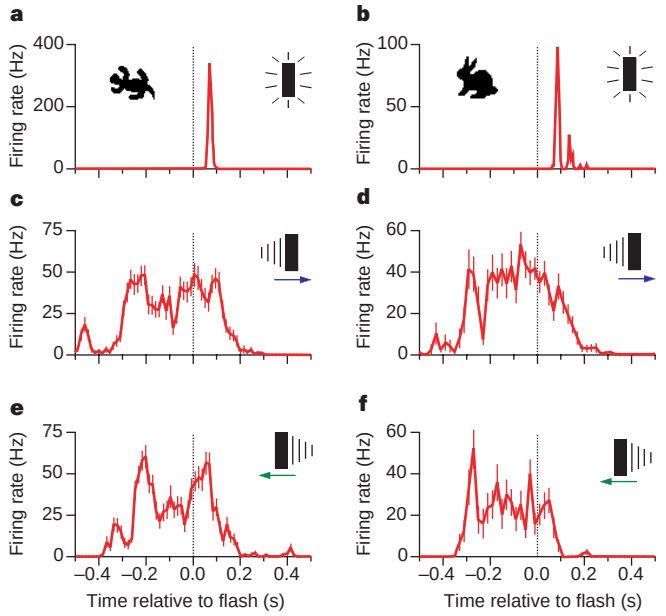

Figure 1 Responses of two ganglion cells to flashed and moving bars. **a**, **c**, **e** Results from a 'fast OFF' ganglion cell in salamander retina; **b**, **d**, **f**, results from a brisk-sustained OFF cell in rabbit retina. **a**, **b**, Firing rate as a function of time after a dark bar (90% contrast, 133 μm width) was flashed for 15 ms on the receptive-field centre. **c**, **d**, Firing rate of the same two cells while the dark bar moved continuously across the retina at 0.44 mm s^{-1}. At time zero, the bar was aligned with the position of the flash in **a** and **b**. **e**, **f**, As in **c**, **d**, but with the bar moving in the opposite direction. Error bars denote standard error across repeated presentations of the stimulus.

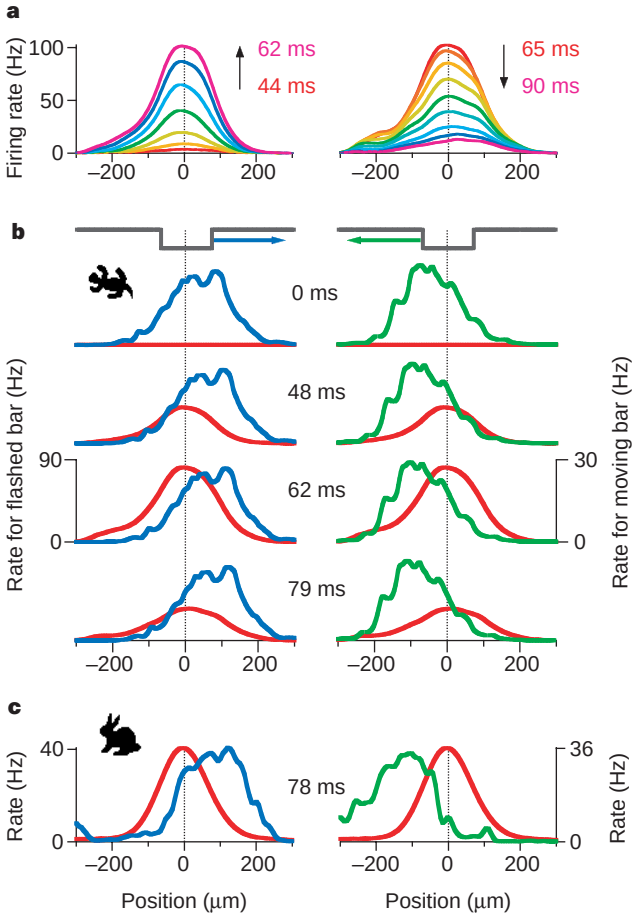

Figure 2 Population response to flashed and moving bars. **a**, Spatial profile of firing in the population of salamander fast OFF ganglion cells in response to a flashed dark bar (90% contrast, 133 μm width, see stimulus trace in **b**) at a series of times after the flash (colour scale, 3 ms steps). **b**, Profile of the population response at four time points following a flashed bar (red, from **a**), and the same bar travelling at 0.44 mm s^{-1} rightward (blue) and leftward (green). At time 0 ms, the moving bars were aligned with the position of the flash; at 62 ms, the flash response was maximal. Curves in **a** and **b** derived from 15 cells. **c**, As in **b**, for the population of brisk-sustained OFF cells in rabbit retina. At 78 ms, the flash response was maximal. Curves derived from six cells.

time delay. In that case, a ganglion cell just ahead of the bar should be strongly excited as the edge begins to enter its receptive-field centre, but then its response gain gets reduced and the firing rate declines even before the edge is half-way across. A well-known component of retinal processing that fits this description is the 'contrast-gain control'[13–15].

Following ref. 16, we incorporated this aspect into a quantitative description of a ganglion cell's light response (Fig. 4). In this scenario, the retina integrates the light stimulus over space and time, with a weighting function $k(x,t)$ given by the ganglion cell's receptive field, and the resulting signal determines the neuron's firing rate. If the stimulus provides strong excitation for an extended period of time, a negative feedback loop reduces the gain at the input and consequently the response to subsequent stimulation[17]. With just four free parameters, this model produced a satisfying account of neural responses throughout the entire contrast series (Fig. 3a). It indicates that the retinal gain is modulated as much as fourfold during passage of the high-contrast bar (Fig. 3b), which pushes the response profile towards the leading edge of the bar. Without contrast-gain control the predicted profile always lagged significantly behind (Fig. 3a).

This explanation indicates that there will be clear limits to what stimuli can be anticipated. For example, if the bar moves fast enough to cross the receptive field before the contrast-gain control sets in, then the peak of the firing profile should lag behind the leading edge. Figure 5a explores these limits, and shows that up to speeds of about 1 mm s^{-1} on the retina, the shape of the firing profile among ganglion cells remained essentially unchanged, with a peak near or ahead of the leading edge. At higher speeds, however, the response profile began to slip significantly behind the leading edge.

This basic relationship was confirmed for several different populations of ganglion cells in both rabbit and salamander (Fig. 5b). The various cell types differed in the extent of anticipation at low speeds, but all began to show a lag in the neural image at speeds of 1–2 mm s^{-1}. In particular, direction selectivity does not play a special role in motion anticipation.

In summary, we have shown that the extrapolation of a moving object's trajectory begins in the retina. In the neural image that the eye transmits to the brain, the moving object is clearly ahead of the corresponding flashed object (Fig. 2). According to a successful model for the ganglion cell's light response (Figs 3, 4), motion anticipation in these populations can be explained on the basis of the spatially extended receptive field, the biphasic temporal response and a nonlinear contrast-gain control. There are several indications that this retinal mechanism contributes strongly to human perception of moving stimuli. First, the requisite components of our model are well documented in many species. In the primate retina, a nonlinear contrast-gain control is found specifically in the M-type ganglion cells[15], neurons that feed the central pathways leading to motion perception[18]. Second, retinal motion extrapolation breaks down at speeds above 1 mm s^{-1} (Fig. 5b). This corresponds well with observations on human subjects: At retinal speeds of 0.3–0.9 mm s^{-1}, perceptual motion extrapolation appeared to compensate for the entire visual delay[5], whereas at speeds of ~4 mm s^{-1} only partial extrapolation was observed[10]. Finally, the retina anticipates high-contrast stimuli more than low-contrast stimuli (Fig. 3), a further departure from ideal extrapolation. Again, this effect has been observed in human psychophysics[9].

In general, an animal is likely to benefit from anticipating the

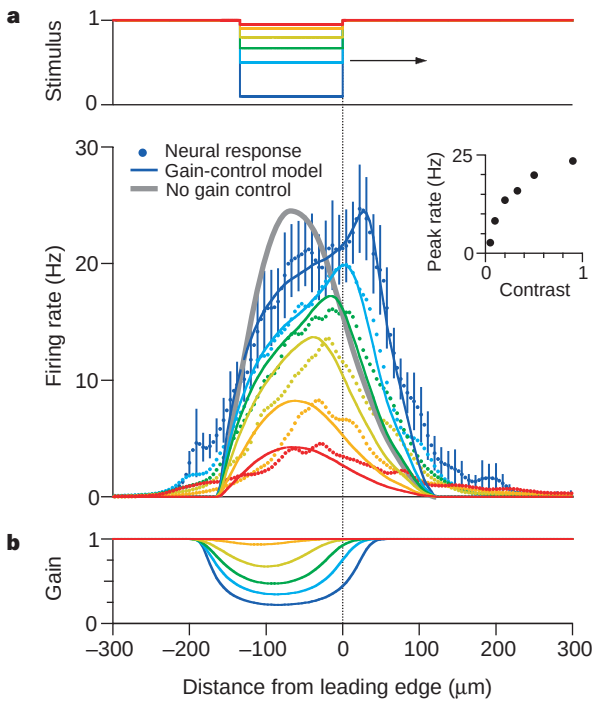

Figure 3 Dependence of motion extrapolation on contrast. **a**, Stimulus with moving dark bars (133 μm width, 0.44 mm s^{-1} speed) of varying contrast: 5, 10, 20, 33, 50 and 90% (see top stimulus traces). Main panel shows the response profile derived from 15 salamander fast OFF ganglion cells (coloured dots), and the predicted response (coloured lines) from a model incorporating contrast-gain control (Fig. 4). Grey line shows the prediction without contrast-gain control. Inset, the peak firing rate of the response profile as a function of the contrast of the bar. Error bars denote standard error, derived from variation among ganglion cells. **b**, Gain variable g of the gain control model (Fig. 4). Model parameters: $\theta = 0$, $\alpha = 85$ Hz, $B = 45$ s^{-1}, $\tau = 170$ ms.

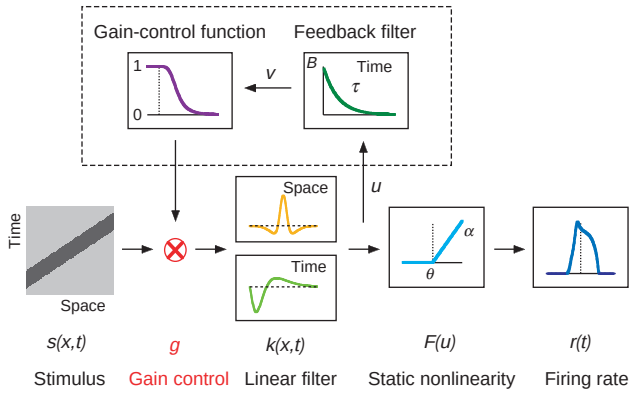

Figure 4 Cascade model for a ganglion cell's light response. The stimulus $s(x,t)$ is multiplied by a gain factor g, convolved with a spatiotemporal filter $k(x,t)$, and rectified by a static nonlinear function $F(u)$ to produce the firing rate $r(t)$. The contrast-gain control mechanism (boxed region) takes the output of the linear filter u, averages it by exponential filtering in time, and uses the result v to set the gain factor g through a decreasing gain control function $g(v)$. Formally,

$$u(t) = g(v)\int_{-\infty}^{\infty} dx \int_{-\infty}^{t} dt'\, s(x,t')k(x,t-t')$$

$$v(t) = \int_{-\infty}^{t} dt'\, u(t')B \exp\left(-\frac{t-t'}{\tau}\right)$$

$$g(v) = \begin{cases} 1 & v < 0 \\ 1/(1+v^4) & v > 0 \end{cases}$$

$$F(u) = \begin{cases} 0 & u < \theta \\ \alpha(u-\theta) & u > \theta \end{cases}$$

The filter $k(x,t)$ is measured (see Methods), and $g(v)$ is taken from a previous, successful model of contrast-gain control in the salamander retina[17]. Thus, the model has four parameters: the threshold θ and slope α of the rectifier $F(u)$, and the amplitude B and time constant τ of the gain control filter.

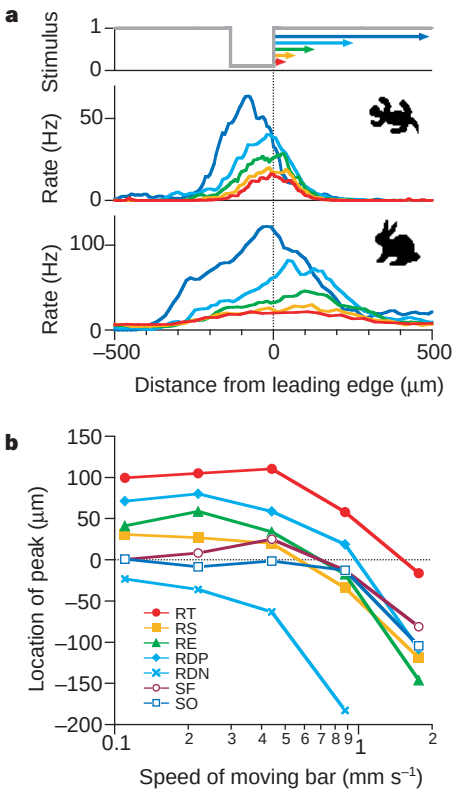

Figure 5 Dependence of motion extrapolation on speed. **a**, Stimulation with moving dark bars (90% contrast, 133 μm width) of varying speed: 0.11, 0.22, 0.44, 0.88 and 1.76 mm s^{-1} (see top stimulus traces). Firing profiles are plotted for salamander fast OFF ganglion cells (middle panel, 19 cells) and rabbit brisk-transient OFF cells (bottom panel, 3 cells). **b**, Motion extrapolation as a function of speed for various populations of ganglion cells. The distance between the peak in the firing-rate profile and the leading edge of the moving bar is plotted as a function of speed; positive numbers indicate that the response profile peaked ahead of the leading edge. The functional types are: salamander, fast OFF (SF, 19 cells); salamander, other OFF (SO, 16 cells); rabbit, brisk-transient OFF (RT, 3 cells); rabbit, brisk-sustained OFF (RS, 6 cells); rabbit, local edge detectors (RE, 4 cells); rabbit, ON/OFF direction-selective cells (5 cells) probed in the preferred direction (RDP) and the null direction (RDN).

future position of an object, for example to pounce on it or to evade it. This is particularly urgent when the primary sensory data are delayed. In principle, this delay could be compensated anywhere within the behavioural loop, even within the motor system that executes the response. However, it is advantageous to perform the correction early, before different sensory pathways merge. For example, in many animals the retina projects directly to the tectum or the superior colliculus, where a visual map of space is overlaid with an auditory map[19,20]. Auditory transduction in hair cells incurs a much shorter delay than phototransduction[21]. If the visual and auditory images of a moving object should align on the target map, the compensation for the delay in the visual pathway must occur within the retina.

It is likely that subsequent stages of the visual system continue this process, possibly by using a similar mechanism. Within the visual cortex we can certainly find the requisite components of the model in Fig. 4: for example, local pooling of excitatory inputs, time-delayed inhibition and mechanisms of nonlinear gain control[22,23]. More generally, there are many instances within the cortex where variables relevant to our behaviour are mapped onto two-dimensional sheets of neurons[24]. If the time course of these variables produces a smooth trajectory of neural activity on the cortical map, then a mechanism such as that described here can predict their future from past observations. □

Methods

Recording. Retinae were obtained from larval tiger salamanders and Dutch belted rabbits. A piece of isolated retina was placed ganglion-cell-layer-down on a multi-electrode array, which recorded spike trains simultaneously from many ganglion cells, as described previously[11,25].

Stimulation. Visual stimuli were generated on a computer monitor and projected onto the photoreceptor layer, as described[25]. All experiments used a background of white light, with a photopic intensity of $M = 11$ mW m^{-2}. Dark bars of intensity B were presented on this background, and the contrast of a bar is defined as $C = (M - B)/M$. A screen pixel of the monitor measured 6.7 μm on the retina, and each video frame lasted 15 ms. Thus, a bar sweeping at 0.44 mm s^{-1} moved by one pixel every video frame. Flashed bars were presented for a single video frame.

Receptive fields. The spatiotemporal receptive fields of all ganglion cells were measured by reverse correlation to randomly flickering stripes[25], orientated parallel to the bars from other experiments. Each of the contiguous 13-μm wide stripes was randomly turned on or off every 30 ms. From ~60 min of recording, we computed for each ganglion cell the average stimulus sequence in the one second preceding an action potential. This reverse correlation is a measure of how the ganglion cell integrates light over space and time. Its time-reverse is the ganglion cell's linear kernel $k(x,t)$ (ref. 26), which can also be interpreted as the effect of a thin line flashed at distance x on the cell's firing rate at time t after the flash[11]. As expected, $k(x,t)$ had a 'Mexican hat' spatial profile, reflecting opposite effects from centre and surround[27], and a biphasic time course (see Fig. 4 and ref. 11).

Cell types. Retinal ganglion cells appear in distinct functional types, and we took care to analyse these subpopulations separately. Salamander cells were classified based on their spatiotemporal receptive fields and on responses to uniform square-wave flashes, as described[28]. Rabbit cells were classified based on the spatiotemporal receptive field and the shape of the spike train's autocorrelation function, following the criteria of ref. 29. Direction-selective cells produced at least tenfold more spikes to one direction of the moving bar than to the opposite direction.

Population activity. The profile of population activity was evaluated along the spatial dimension perpendicular to the bars. Each cell's position was defined as the middle of its receptive field, determined by fitting a spatial gaussian to the centre lobe of the kernel $k(x,t)$. To estimate the population response to a flashed bar, the flash was repeated 75 times in each of 15 locations, separated by 33 μm. For each flash location and each ganglion cell, the firing rate following the flash (Fig. 1a, b) was calculated using a time bin of 2 ms. To compose the firing profile at a given time after the flash, each ganglion cell's firing rate was plotted against the cell's position relative to the flashing line. This plot was smoothed by convolution with a gaussian of standard deviation 20 μm. To estimate the population response to a moving bar, the stimulus was repeated 50 times, and each ganglion cell's firing rate computed as for flashes, but with a time bin of 15 ms. Then the firing rate was plotted against the distance from the bar, and averaged over all cells.

Received 11 December 1998; accepted 2 February 1999.

1. Maunsell, J. H. & Gibson, J. R. Visual response latencies in striate cortex of the macaque monkey. *J. Neurophysiol.* **68,** 1332–1344 (1992).
2. Lennie, P. The physiological basis of variations in visual latency. *Vision Res.* **21,** 815–824 (1981).
3. Schnapf, J. L., Kraft, T. W. & Baylor, D. A. Spectral sensitivity of human cone photoreceptors. *Nature* **325,** 439–441 (1987).
4. De Valois, R. L. & De Valois, K. K. Vernier acuity with stationary moving Gabors. *Vision Res.* **31,** 1619–1626 (1991).
5. Nijhawan, R. Motion extrapolation in catching. *Nature* **370,** 256–257 (1994).
6. Khurana, B. & Nijhawan, R. Extrapolation or attention shift? *Nature* **378,** 566 (1995).
7. Nijhawan, R. Visual decomposition of colour through motion extrapolation. *Nature* **386,** 66–69 (1997).
8. Baldo, M. V. & Klein, S. A. Extrapolation or attention shift? *Nature* **378,** 565–566 (1995).
9. Purushothaman, G., Patel, S. S., Bedell, H. E. & Ogmen, H. Moving ahead through differential visual latency. *Nature* **396,** 424 (1998).
10. Whitney, D. & Murakami, I. Latency difference, not spatial extrapolation. *Nature Neurosci.* **1,** 656–657 (1998).
11. Smirnakis, S. M., Berry, M. J., Warland, D. K., Bialek, W. & Meister, M. Adaptation of retinal processing to image contrast and spatial scale. *Nature* **386,** 69–73 (1997).
12. Jacobs, A. L. & Werblin, F. S. Spatiotemporal patterns at the retinal output. *J. Neurophysiol.* **80,** 447–451 (1998).
13. Shapley, R. M. & Victor, J. D. The effect of contrast on the transfer properties of cat retinal ganglion cells. *J. Physiol.* **285,** 275–298 (1978).
14. Sakai, H. M., Wang, J. L. & Naka, K. Contrast gain control in the lower vertebrate retinas. *J. Gen. Physiol.* **105,** 815–835 (1995).
15. Benardete, E. A., Kaplan, E. & Knight, B. W. Contrast gain control in the primate retina: P cells are not X-like, some M cells are. *Visual Neurosci.* **8,** 483–486 (1992).
16. Victor, J. D. The dynamics of the cat retinal X cell centre. *J. Physiol.* **386,** 219–246 (1987).

17. Crevier, D. W. & Meister, M. Synchronous period-doubling in flicker vision of salamander and man. *J. Neurophysiol.* **79,** 1869–1878 (1998).
18. Merigan, W. H. & Maunsell, J. H. How parallel are the primate visual pathways? *Annu. Rev. Neurosci.* **16,** 369–402 (1993).
19. Sparks, D. L. Translation of sensory signals into commands for control of saccadic eye movements: role of primate superior colliculus. *Physiol. Rev.* **66,** 118–171 (1986).
20. Knudsen, E. I. Auditory and visual maps of space in the optic tectum of the owl. *J. Neurosci.* **2,** 1177–1194 (1982).
21. Corey, D. P. & Hudspeth, A. J. Response latency of vertebrate hair cells. *Biophys. J.* **26,** 499–506 (1979).
22. Carandini, M., Heeger, D. J. & Movshon, J. A. Linearity and normalization in simple cells of the macaque primary visual cortex. *J. Neurosci.* **17,** 8621–8644 (1997).
23. Abbott, L. F., Varela, J. A., Sen, K. & Nelson, S. B. Synaptic depression and cortical gain control. *Science* **275,** 220–224 (1997).
24. Knudsen, E. I., du Lac, S. & Esterly, S. D. Computational maps in the brain. *Annu. Rev. Neurosci.* **10,** 41–65 (1987).
25. Meister, M., Pine, J. & Baylor, D. A. Multi-neuronal signals from the retina: acquisition and analysis. *J. Neurosci. Methods* **51,** 95–106 (1994).
26. Hunter, I. W. & Korenberg, M. J. The identification of nonlinear biological systems: Wiener and Hammerstein cascade models. *Biol. Cybern.* **55,** 135–144 (1986).
27. Rodieck, R. W. Quantitative analysis of cat retinal ganglion cell response to visual stimuli. *Vision Res.* **5,** 583–601 (1965).
28. Warland, D. K., Reinagel, P. & Meister, M. Decoding visual information from a population of retinal ganglion cells. *J. Neurophysiol.* **78,** 2336–2350 (1997).
29. Devries, S. H. & Baylor, D. A. Mosaic arrangement of ganglion cell receptive fields in rabbit retina. *J. Neurophysiol.* **78,** 2048–2060 (1997).

Acknowledgements. We thank J. Keat for assistance in generating the visual stimulus, and H. Berg and T. Holy for comments on the manuscript. This work was supported by a NRSA to M.B. and a grant from the NIH and a Presidential Faculty Fellowship to M.M.

Correspondence and requests for material should be addressed to M.J.B. (e-mail: berry@biosun.harvard.edu).

A new cellular mechanism for coupling inputs arriving at different cortical layers

Matthew E. Larkum, J. Julius Zhu & Bert Sakmann

Abt. Zellphysiologie, Max-Planck-Institut für Medizinische Forschung, Jahnstrasse 29, D-69120 Heidelberg, Germany

Pyramidal neurons in layer 5 of the neocortex of the brain extend their axons and dendrites into all layers. They are also unusual in having both an axonal and a dendritic zone for the initiation of action potentials[1–6]. Distal dendritic inputs, which normally appear greatly attenuated at the axon, must cross a high threshold at the dendritic initiation zone to evoke calcium action potentials[1,7] but can then generate bursts of axonal action potentials. Here we show that a single back-propagating sodium action potential generated in the axon[8] facilitates the initiation of these calcium action potentials when it coincides with distal dendritic input within a time window of several milliseconds. Inhibitory dendritic input can selectively block the initiation of dendritic calcium action potentials, preventing bursts of axonal action potentials. Thus, excitatory and inhibitory postsynaptic potentials arising in the distal dendrites can exert significantly greater control over action potential initiation in the axon than would be expected from their electrotonically isolated locations. The coincidence of a single back-propagating action potential with a subthreshold distal excitatory postsynaptic potential to evoke a burst of axonal action potentials represents a new mechanism by which the main cortical output neurons can associate inputs arriving at different cortical layers.

Triple recordings were made on two sites of the apical dendrites and the somata of layer-5 pyramidal neurons (Fig. 1a). Subthreshold excitatory-postsynaptic-potential(EPSP)-shaped potentials in the distal apical dendrites were strongly attenuated as they spread to the soma (Fig. 1b). Back-propagating action potentials from the axon reached the distal dendritic tufts (Fig. 1c) where they caused an influx[9] of Ca^{2+}. However, single sodium action potentials (Na^+-APs) initiated in the axon do not evoke a calcium action potential (Ca^{2+}-AP) in the dendrite[1,3,4,6–9] (Fig. 1c). The combination of a subthreshold EPSP-shaped distal dendritic potential (Fig. 1b) and a back-propagating action potential (Fig. 1c) elicited a Ca^{2+} and Na^+ action potential complex in the dendrite (Fig. 1d; $n = 27$) that resulted in 2–3 (2.2 ± 0.1; frequency: 101 ± 8 Hz) Na^+-APs at the soma. This back-propagating action potential activated Ca^{2+} spike firing (BAC firing) was evoked with 1.1 nA (± 0.1 nA) peak current injection at a distal dendritic location (average 693 ± 18 μm from soma). This was only half the current amplitude ($49 \pm 4\%$; $n = 27$) that evoked a comparable Ca^{2+}-AP in the absence of a back-propagating action potential (Fig. 1e). In the neuron shown in Fig. 1d, the current needed was only 0.3 nA (25% of threshold). The threshold dendritic current for BAC firing was typically less than the threshold for eliciting a Na^+-AP using the same-shaped current injection at the soma, suggesting that the dendritic component requires fewer synaptic inputs than are needed for axonal Na^+-APs (possibly less than ten inputs[1]).

The optimal time for eliciting a Ca^{2+}-AP with dendritic current injection was 3–7 ms after the somatic action potential. At threshold, the time interval (Δt) for evoking BAC firing was very narrow. Here, dendritic current injection given at Δt values of 3, 7 and 11 ms (Fig. 2a–c, respectively) elicited BAC firing only at $\Delta t = 7$ ms. The average threshold for BAC firing was measured at 5-ms time intervals (Fig. 2d; $n = 8$) and revealed a sharp minimum at $\Delta t = 5$ ms. The threshold for BAC firing rose sharply for delays of over 5 ms, and was even higher than the threshold for eliciting a Ca^{2+}-AP in the absence of a back-propagating action potential for delays of 10–130 ms. This shows that the generation of a Ca^{2+}-AP is greatly facilitated if the dendritic EPSP and axonal action potential

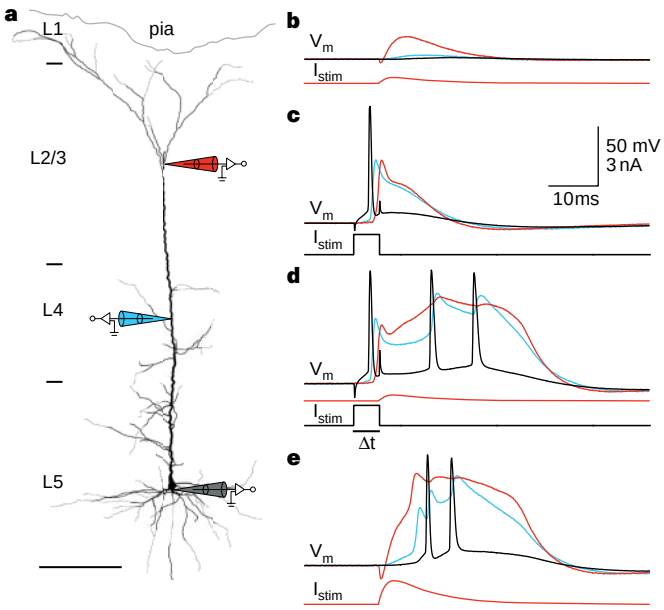

Figure 1 Coupling of a back-propagating action potential (AP) with distal subthreshold current injection. **a**, Reconstruction of a biocytin-filled pyramidal neuron, with the recording pipette positions shown symbolically (770 μm from soma in red, 400 μm from soma in blue and one at the soma in grey). Cortical layers are indicated on the left. Scale bar, 200 μm. **b**, Current injection of 0.3 nA (peak amplitude) at the distal pipette (red trace, bottom) in the shape of an EPSP produced a signal of only 1.4 mV at the soma. It did not reach threshold for either a Ca^{2+}-AP or a Na^+-AP. I_{stim} refers to traces representing current injected and V_m to potential recorded. Positive current causes intracellular depolarization. The colour indicates the corresponding electrode in the diagram. **c**, Threshold current injection at the soma (black trace labelled I_{stim}) evoked an AP that reduced in amplitude but increased in width in the dendrite. **d**, BAC firing. The combination of these injections of current (used in **b** and **c**) separated by an interval (Δt) of 5 ms evoked a burst of APs following the onset of the Ca^{2+}-AP in the distal dendrite. (Δt, time between the onset of each pulse.) Scale bars in **c** also apply to **b** and **d**. **e**, A similar dendritic Ca^{2+}-AP could be evoked by a larger (1.2 nA) current injection alone at the distal dendritic electrode, as shown previously[1].